# ABSTRACT

LUKE, WILLIAM HARRISON. Synthesis and Characterization of a ZnO-Cu Thermoelectric Nano-composite. (Under the direction of Dr. Jon-Paul Maria.)

Thermoelectric materials have slowly been developed to improve the efficiency of thermoelectric devices by using the effect of nanoscale structures within the materials. Additionally, new classes of materials are being utilized to meet the needs of more specialized thermoelectric applications. In particular, a Zinc oxide (ZnO) matrix with copper (Cu) nanoparticles offers a possibility for a thermally and chemically stable thermoelectric material at high temperatures.

This thesis reports an investigation into the effectiveness of a ZnO-Cu nano-composite, from synthesis to bulk thermal property measurements. A variety of compositions of ZnO and CuO powders were processed into bulk pellets, which were then reduced in specific gas atmospheres to achieve the selective reduction of CuO from the material. The effectiveness of this reduction was examined using x-ray diffraction, which showed a complete reduction of CuO to Cu metal, while maintaining a ZnO matrix. Samples were then prepared for transmission electron microscopy to study the structure of the ZnO-Cu system. TEM analysis showed regularly dispersed rod-shaped particles approximately 150 nm in length and 30 nm in width, with distribution and particle size reducing with decreased Cu concentration. Preliminary thermal conductivity measurements of the 1 and 5 volume percent Cu

samples show thermal conductivities of 17.3 W/m/K and 14.8 W/m/K respectively, a significant reduction from the pure ZnO conductivity of approximately 52 W/m/K.

# Synthesis and Characterization of a ZnO-Cu Thermoelectric Nano-composite

by
William Harrison Luke

A thesis submitted to the Graduate Faculty of
North Carolina State University
in partial fulfillment of the
requirements for the Degree of
Master of Arts

Materials Science and Engineering

Raleigh, North Carolina

2013

APPROVED BY:

| | |
|---|---|
| _____ | _____ |
| Dr. Elizabeth Dickey | Dr. Mark Losego |

_____
Dr. Jon-Paul Maria
Chair of Advisory Committee

## BIOGRAPHY

William Harrison Luke was born on March 25, 1988 to parents Susan and Larry Luke in Madison, Mississippi. From a young age he was fascinated by the world around him and wanted to learn how and why things behaved they way they did. This fascination grew throughout his childhood, ultimately leading him to pursue a degree in engineering.

William attended Mississippi State University for his Bachelor's studies in mechanical engineering. While his love of science was great, it was not focused in any one area. Much of his time at MSU was spent finding a field that piqued his interest. After working in a number of areas, including computational fluid dynamics with Dr. Keith Walters, William finally found his calling in materials research, with a focus on applied engineering.

So he moved to North Carolina to purse his Master's degree in North Carolina State University's Department of Materials Science & Engineering. Eventually, William joined Dr. Jon-Paul Maria's group and began that group's work on thermoelectric research. William successfully defended his Master's thesis on June 21$^{st}$, 2013.

## ACKNOWLEDGEMENTS

None of this work would have been possible without the assistance and support of many people. First, a big thanks to Dr. Jon-Paul Maria for providing the time, support, and equipment for all of this work. Also, thank you to Dr. Patrick Hopkins at the University of Virginia for his help with thermal measurements for this study. Thank you to Dr. James LaBeau and his group, specifically Adedapo Oni and Houston Dycus, as well as Lindsay Hussey for their assistance during TEM sample preparation and analysis. And another big thanks to Edna Deas for her help in keeping everything in order and on time.

Another thank you to all the current and past group members, who were always able to provide assistance and support, as well as a friendly environment in and out of the lab: Peter Lam, Beth Paisley, David Hook, David Harris, Edward Sachet, Chris Shelton, Alex Smith, Ed Mily, Xiao Yu Kang, and Tina Rost.

Of course none of this was possible without the support of family. I'm eternally grateful my parents, Susan and Larry Luke, for raising me to love to learn and enjoy the wonders of the world around me. And the biggest thanks to my wife, Christi Luke, for her constant support and ability to keep me focused and calm throughout the course of my studies.

## TABLE OF CONTENTS

## LIST OF FIGURES

# CHAPTER 1

# INTRODUCTION

As the world's energy demands continue to increase and cheap, sustainable resources for producing energy become increasingly scarce, new methods of energy conversion need to be developed and greatly improved upon to meet society's future requirements. These developments are not likely to be momentous new discoveries, but instead incremental improvements to current technologies. Solar cells, wind turbines, geothermal generators, and the like, are some existing technologies that are experiencing this evolution, and are now used in many large-scale, practical applications. However, a prime example of one such technology currently used in a few niche applications, is thermoelectric devices.

Like many of these other renewable energy systems, thermoelectric systems are able to generate electricity from an under-utilized phenomenon, in this case a temperature gradient. When in the presence of a temperature gradient, an electric potential is produced in the material, which causes charge carriers to migrate to one end of the material creating an electric potential. This type of system is typically called a thermoelectric generator. The reverse of this process is also useful for practical applications in devices known as thermoelectric refrigerators. When an electric potential is induced in a thermoelectric material, a temperature gradient is produced which can be used to cool the surrounding environment.

Using thermoelectric generators and refrigerators, new systems for power generation and cooling can be created that offer a variety of benefits, which include the durability of a solid-state system as well as the stability of a system with no moving parts [1]. However, the current state of thermoelectric technologies is simply not developed enough to compete with conventional systems. Significant improvements to the efficiency of thermoelectric systems will need to be made before they can be implemented in new areas.

For power generation applications in particular, there are innumerable situations where existing technologies produce considerable amounts of heat. This heat is often an undesirable but accepted by-product of the physics of these technologies. When thermoelectric materials are improved, devices can be made that will directly harvest this wasted heat and convert it into electricity. One particularly intriguing application for this would be in automobiles. A number of sources of waste heat in a vehicle from the engine to the exhaust could be used to charge batteries or run on-board electronics, hence increasing the total efficiency of the vehicle. Potential sources for thermoelectric harvesting are large power plants and other industrial processes which often exhaust large amounts of heat during normal operations, as well as solar power panels which often are unable to utilize the low energy radiation they absorb. With more efficient thermoelectric generators, they could provide a primary source of power for a variety of situations. Currently, radioisotope thermoelectric generators, which capture the heat from radioactive decay to produce power, are used in many space applications, and increasing their

effectiveness would extend humanity's reach into outer space. Something as simple as running efficient lighting from the heat of a stove would provide an easy source of electricity to a large number of people around the world.

Just as new applications for power generation can be found with improved efficiency, thermoelectric refrigeration would become more relevant with better thermoelectric materials. Primarily, these new materials would improve current devices, especially in the realm of scientific instruments. Many systems that require cooling are often limited by the heat they generate. In particular, heat accumulation is space-based systems is a constant worry. Using thermoelectric refrigeration devices to help quickly transfer thermal energy from critical areas, such as electrical components or sun facing regions, would allow for these systems to run at safer limits. In general, the benefits of an improved thermoelectric refrigerator would allow for more powerful or more sensitive components to be used in a large number of settings, leading to faster or more accurate results in many different areas of research.

The current direction of thermoelectric research is focused on two areas: searching for new bulk materials, and improving existing materials through low-dimensional systems. Bulk materials research has most prominently focused on phonon-glass/electron-crystal (PGEC) materials. These materials would thermally behave like a glass with low conductivity while, at the same time, electronically act like a crystal with high conductivity. This is achieved by introducing weakly bound atoms within the crystal structure that scatter phonons. Research in low-

dimensional materials is further broken down into two areas. First, the effect of nanoscale constituents introduced into the material that would enhance the power factor of the thermoelectric figure-of-merit (which will be discussed in more detail in Chapter 2). Second, the selective reduction of thermal conductivity over electrical conductivity is achieved by the many internal interfaces found in the nanostructures, due to the differences in their respective scattering lengths [2].

In the vast majority of thermoelectric systems, the thermal-electric energy conversion efficiency is increased at higher temperatures. However, many of the thermoelectric materials used for high temperature applications are not stable at their operating temperatures and must be coated in a stable compound to prevent exposure to the atmosphere [3,4]. Thus, new materials, such as various silicides, are being investigated for these high temperature situations. However, there are many oxide materials which are very stable at high temperatures in air and have received less attention in the past [1]. In particular, zinc oxide (ZnO), an n-type semiconducting oxide, shows promise as a high-temperature (>700°C) thermoelectric material. It has a high melting point (~1800°C), good chemical stability, and high electrical conductivity [5]. More importantly and its thermoelectric properties could readily be improved and controlled via doping [6].

The purpose of this study is to provide a review of current thermoelectric materials research and investigate the production of bulk ZnO samples doped with Cu-metal nanoparticles through the selective reduction of CuO. The effects of different processing techniques and parameters for this reduction will be explored

using X-ray diffractometry. The subsequent bulk samples will be examined using a transmission electron microscope to determine the distribution and morphology of the Cu nanoparticles. The remainder of this thesis is arranged as follows: Chapter 2 will provide an overview of the various aspects of the thermoelectric phenomenon. Chapter 3 will review the state-of-the-art for thermoelectric materials, and then investigate some of the methods for improving thermoelectric materials. Chapter 4 will describe the methodology of this investigation. Chapter 5 will show the results of this study and discuss their effects. Finally, Chapter 6 will contain concluding remarks and potential areas for future work.

# CHAPTER 2

# THERMOELECTRIC PHENOMENON

Like many scientific breakthroughs, the discovery of the thermoelectric phenomenon was not the product of a single researcher. For thermoelectrics, it took the work of three individuals, Thomas Seebeck, Jean Charles Peltier, and William Thomson, to describe the fundamental components of this effect. These components are the Seebeck Effect, Peltier Effect, and Thomson Effect with these individual effects combined in the Kelvin Relationships. Finally, the thermoelectric figure-of-merit was later developed as a means to quantitatively compare thermoelectric materials.

## Section 2.1: Seebeck Effect

In 1821, the Baltic German physicist Thomas Johann Seebeck reported his observations of a compass needle placed in the vicinity of a closed loop of two dissimilar conductors, when one of the junctions was heated, producing a voltage. While he falsely concluded that the interaction was a magnetic phenomenon, he did go on to investigate a wide variety of other materials for this interaction, including materials now classified as semiconductors. Ultimately, this interaction was called the Seebeck effect. Seebeck essentially stopped his research at this point, but had he continued on this line of study, he could have made a device with the materials

he discovered and created a thermoelectric power generator of comparable efficiency to other power generators of his day [7]

As briefly mentioned previously, the Seebeck effect is the production of an electromotive force across a material when in the presence of a temperature differential. In a conducting material of finite dimensions with a temperature gradient across the material, charge carriers will generally travel from the hot side to the cool side of the material until an equilibrium electrical potential is reached. This effect illustrated in Figure 2.1. Further increasing the temperature of the hot side will increase the number of charge carriers that to the cool side, establishing a higher potential difference.

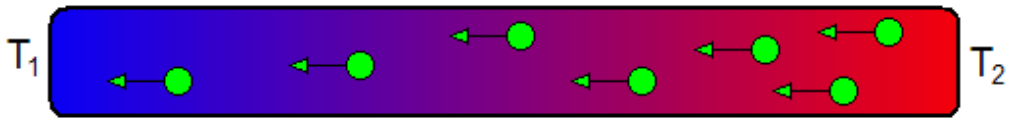


Figure 2.1. In this example, $T_2 > T_1$, and the green circles are the charge carriers. The temperature gradient causes these charge carriers (electrons or holes depending on the material) to move toward the cool side and establish a new equilibrium potential in the material.

To describe this effect, a fundamental electronic transport property called the Seebeck coefficient, S, was derived. This coefficient is defined as the ratio of the electromotive force to the temperature differential. Fundamentally, the Seebeck coefficient measures the entropy transported with a charge carrier as it moves through the material, divided by the carrier's charge [8]. More practically, the

Seebeck coefficient is measured by creating a thermocouple and measuring the voltage difference across the junction and dividing by the temperature difference, as seen in Equation 1,

$$S = \frac{V}{\Delta T} \tag{1}$$

A functional thermocouple, shown in Figure 2.2, is created by putting two dissimilar conductors electrically in series and thermally in parallel. When the temperature gradient is applied, a voltage is produced between points C and D. If the temperatures, $T_1$ and $T_2$, and the voltage across C and D are known, then the Seebeck coefficient can be calculated. When measured this way, the coefficient is a differential coefficient, $S_{ab}$, between the two materials A and B.

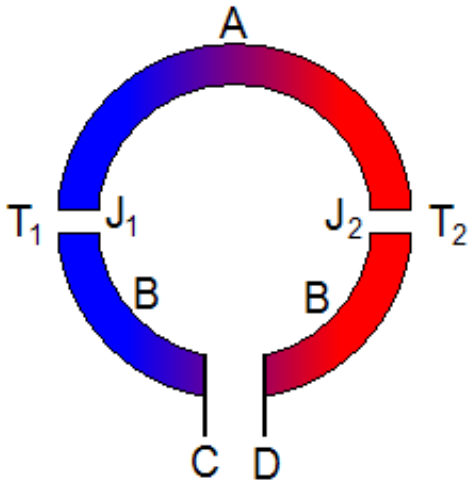


Figure 2.2. A basic thermocouple exhibiting the Seebeck effect. A and B are two dissimilar conducting materials which make an acceptor/donor pair. $J_1$ and $J_2$ are the junctions between the materials and are held at temperatures $T_1$ and $T_2$. This causes a voltage to form across points C and D

The sign of the Seebeck coefficient is determined by the direction of current flow, which is determined by the direction of the temperature gradient. If $T_2$ is greater than $T_1$, the current will flow in the clockwise direction giving a positive Seebeck coefficient. If the gradient is reversed, current will flow counter-clockwise and the sign will be negative.

However, a direct measurement of the Seebeck coefficient is not routinely done, and when performed must be performed very carefully. Since all conducting materials exhibit some degree of a thermoelectric effect, the exception being superconductors below their transition temperature, any measurement would be influenced by the electrodes of the measuring device. Also, when measured with a thermocouple, the relative nature of the Seebeck coefficient must be noted, so proper comparisons can be made [9].

**Section 2.2: Peltier Effect**

The next breakthrough came 12 years later from French physicist Jean Charles Peltier. In a similar experimental setup, Peltier noticed a temperature change in the junction between the dissimilar conductors when a current passed through the junction. Like Seebeck, Peltier failed to grasp the fundamental nature of his observations, and did not make the connection to Seebeck's findings, even though he used this phenomenon in some of his experiments as weak current sources. This complementary effect was named the Peltier effect, and was further

explained in 1838, when Lenz concluded that heat can be absorbed or generated at the junction depending on the direction of current flow [7].

Instead of producing an electromotive force from a temperature gradient, a gradient is produced by a flow of current through the thermocouple, heating one junction while cooling the other. The ratio of the current flow, I, to the heating rate, q, defines the Peltier coefficient, π, as shown in Equation 2.

$$\pi = \frac{I}{q} \tag{2}$$

To qualitatively describe this effect, if current flows clockwise around a thermocouple circuit (see Figure 2.3), then one junction will be heated at rate q, while the other will cooled at a rate –q. The coefficient is defined as positive if $J_1$ is heated and $J_2$ is cooled [9].

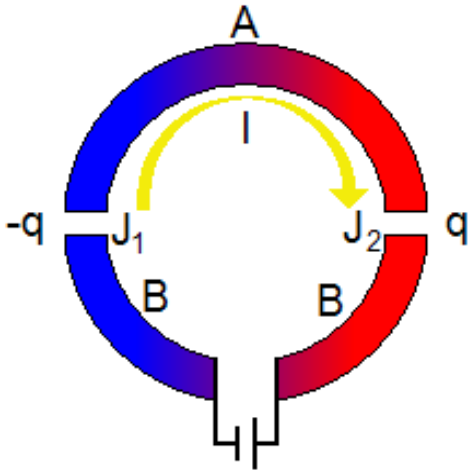


Figure 2.3. A thermocouple exhibiting the Peltier effect. A clockwise current, I, flows through two thermoelectric materials, A and B. $J_1$ experiences a cooling rate of –q, while $J_2$ heats at a rate of q. In this case, a temperature gradient is created by an electric potential.

**Section 2.3: Thomson Effect and Kelvin Relationships**

Little progress was made in the field of thermoelectrics due to the more intriguing discoveries being made in the area of electromagnetism at this time. A small revival of interest occurred in 1851 when William Thomson (better known as Lord Kelvin) discovered the third component of the thermoelectric phenomenon and established the relationship between the Seebeck and Peltier effects. This final effect, called the Thomson effect, describes the heating or cooling of a homogeneous conductor when a current passes through it in the presence of a temperature gradient.

When the temperature difference is small, the Thomson effect is defined by the following equation:

$$q = \beta I \Delta T \tag{3}$$

where q is the heat rate, β is the Thomson coefficient, I is the current, and ΔT is the temperature difference. Typically, the Thomson effect is only accounted for in the cases where the thermal gradient is small. However, it should not be neglected for detailed calculations.

In addition to predicting and discovering the Thomson effect, Lord Kelvin also connected the three thermoelectric coefficients together in what are known as the Kelvin relationships:

$$S_{ab} = \frac{\pi_{ab}}{T} \tag{4}$$

$$\frac{dS_{ab}}{dT} = \frac{\beta_a - \beta_b}{T} \tag{5}$$

Equation 4 relates the Seebeck and Peltier coefficients, and Equation 5 relates the Seebeck and Thomson coefficients. Note that the coefficients used are relative to the specific materials used during the experimental measurements [9].

**Section 2.4: Thermoelectric Figure-of-Merit**

This field received little attention for another long period, until the beginning of the 20$^{th}$ century. Around this time another physicist, Edmund Altenkirch, developed a comprehensive theory of thermoelectric generation and refrigeration and showed that good thermoelectric materials should have large Seebeck coefficients and low thermal conductivity to retain the heat at a junction, in addition to a low electrical resistance to minimize Joule heating, or the resistive heating produced when a current passes through a material [7]. Although the three thermoelectric effects were well defined and related to one another, they did not provide a useful measure for comparison between different materials. The most practical way to evaluate these materials, as shown by Altenkirch, is by comparing their thermoelectric efficiency. In general terms, the efficiency of a simple thermocouple, $\Phi$, is the energy supplied to the load divided by the heat absorbed at the hot junction. Assuming the electrical conductivities, thermal conductivities, and Seebeck coefficients of the two materials are constant, and that the contact resistances are negligible compared to the total resistance, this efficiency can be expressed as

$$\phi = \frac{I^2 R}{S_{ab} I T_H + \lambda'(T_H - T_C) - \frac{1}{2} I^2 R} \tag{6}$$

where λ' is the thermal conductance of the materials in parallel, R is the series resistance of the materials, and $T_H$ and $T_C$ are the hot and cold temperatures respectively. While some of these parameters may vary as a function of temperature, this simple expression can still be employed if approximate averages of values for these parameters over the temperature range are used.

This efficiency is a function of the ratio of the load resistance to the sum of the thermocouple resistance, and at maximum power Equation 6 can be rewritten as

$$\phi_P = \frac{T_H - T_C}{\frac{3T_H}{2} + \frac{T_C}{2} + \frac{4}{Z_c}} \tag{7}$$

where Z is the figure-of-merit of the thermocouple. This gives a maximum efficiency

$$\phi_{\max} = \eta_c \gamma \tag{8}$$

where $\eta_c$ is the Carnot efficiency

$$\eta_c = \frac{T_H - T_C}{T_H} \tag{9}$$

and

$$\gamma = \frac{\sqrt{1 + Z_c T_{avg}} - 1}{\sqrt{1 + Z_c T_{avg}} + \frac{T_c}{T_H}} \tag{10}$$

and the figure-of-merit is defined as

$$Z_c = \frac{S_{ab}^2}{R\lambda'} \tag{11}$$

Thus, the maximum efficiency is a product of the Carnot efficiency, and γ, which contains the parameters of the materials.

In practice, the geometries of the two materials are typically matched to minimize heat absorption, and the two materials of the thermocouple have roughly similar material constants. This allows the figure-of-merit to be written in a more useful form:

$$Z = \frac{S^2\sigma}{\lambda} \tag{12}$$

where σ is the electrical conductivity and λ is the thermal conductivity. The $\sigma S^2$ term is often referred to as the electrical power factor [9] Also, the units of this figure-of-merit are $K^{-1}$, so Equation 12 is often multiplied by the temperature in order to produce a non-dimensional version of the figure-of-merit, ZT, given by

$$ZT = \frac{S^2\sigma}{\lambda}T \tag{13}$$

The difficulty of improving ZT in most materials is that all of the parameters in the above equation are linked together, and so independently manipulating one variable at a time is impossible. For example, one possible way to increase ZT would be to reduce the thermal conductivity. The total thermal conductivity of a material, λ, has contributions from the lattice vibrations, $\lambda_l$, as well as from the charge carriers moving through the lattice, $\lambda_e$, as shown in Equation 14.

$$\lambda = \lambda_e + \lambda_l \tag{14}$$

As carrier concentrations in the material increase, the carrier contribution to the total thermal conductivity increases. For semiconductors however, thermal conductivity is dominated by lattice vibrations and in thermoelectric materials only one third of total conductivity is contributed by charge carriers [9]. Ideally, reducing the lattice vibrations would contribute quite a large amount to increasing ZT. Unfortunately, this is prohibited by the Wiedmann-Franz law [10], which is defined in Equations 15 and 16

$$\lambda = (\frac{3k_B^2}{2e^2})\sigma T \qquad \text{Equation 15}$$

$$\lambda = L\sigma T \qquad \text{Equation 16}$$

where λ is the total thermal conductivity, $k_B$ is Boltzmann's constant, e is the charge of an electron, σ is the electrical conductivity, L is the Lorenz factor, and T is the temperature. From these equations, it is clear that the thermal conductivity and electrical conductivity are directly related to each other and any decrease in thermal conductivity would result in a decrease in electrical conductivity, reducing any possible benefit to ZT. Figure 2.4 shows this problem graphically.

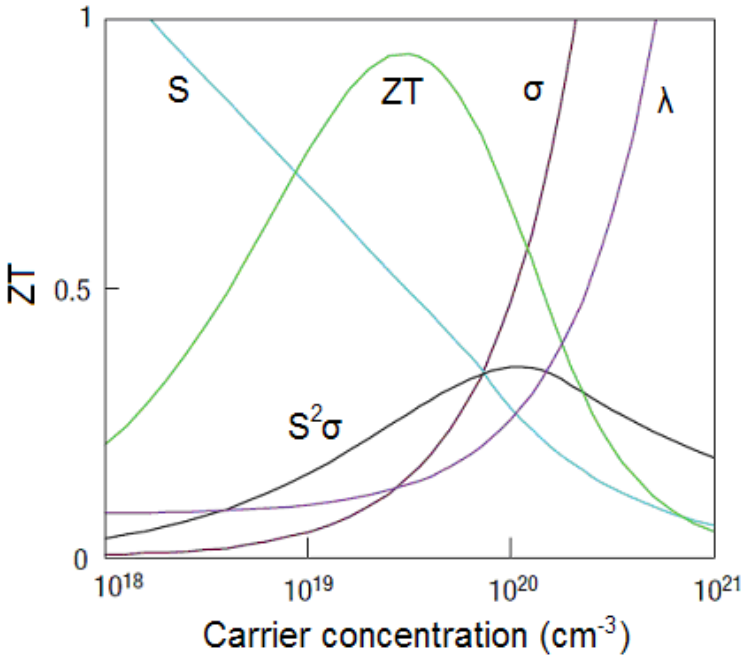


Figure 2.4. This illustrates the intertwined nature of the constituents of the thermoelectric figure-of-merit [6].

For the given material represented (in this case $Bi_2Te_3$) there exists an optimized value for the maximum power factor and maximum ZT. Any significant change from these optimized parameters would reduce ZT and the efficiency of the material, so improvements must be carefully designed.

# CHAPTER 3

# THERMOELECTRIC MATERIALS

Like the work done in developing the theory of thermoelectric phenomena, research into materials which exhibit good thermoelectric properties has been a slow process with many long periods of little to no advancement. This has primarily been due to the difficulties in controlling the components of the figure-of-merit, as well as lack of interest in the field in the face of other discoveries being made in the wider electromagnetism fields. After the initial discovery of the thermoelectric phenomena, very little research was done to discover materials that specifically exhibited good thermoelectric properties. This changed in the 1950s once the basic theory of thermoelectric materials became well established, the heavily doped semiconductors were accepted as ideal materials of interest, and $Bi_2Te_3$ was developed for commercial applications. These three advancements opened the way for the modern thermoelectric industry.

After this initial burst of activity, only slight gains were made in improving the thermoelectric figure-of-merit, ZT, in the next thirty years, with $Bi_2Te_3$ alloys remaining the best materials used in devices with ZTs approximately equal to 1 in nearly all cases [11]. In the mid 1990s, a resurgence of interest began with theoretical predictions suggesting that nanostructured materials could provide much higher efficiencies and proof-of-principle work began in this area. Also, the slow

gains in traditional research into new, complex bulk materials found that higher efficiencies could be achieved [6].

Most of the current thermoelectric materials can be divided in to two broad categories: intermetallic compounds and complex crystals. However, a novel class of thermoelectric materials, metal oxides, has recently received more attention in research circles. The remainder of this chapter will discuss these three categories of materials, as well as some of the methods used and theorized for improving the thermoelectric performance of these materials using nanoscale structures.

**Section 3.1: Intermetallic compounds**

Inter-metallic alloys were some of the first successful thermoelectric materials to be discovered, the most notable of which is $Bi_2Te_3$, ($ZT \approx 1$), which has been the primary thermoelectric material for commercial applications since the 1950s. Two other common compounds, PbTe and $Si_{1-x}Ge_x$, will be discussed in this section.

$Bi_2Te_3$ is a narrow-gap semiconductor that can be alloyed with Sb to become a p-type semiconductor and with Se for n-type. The crystal structure of $Bi_2Te_3$ is a layered structure held together by van der Waals interactions. Each layer is perpendicular to the c-axis of the crystal and follows the sequence: $Te^{(1)} – Bi – Te^{(2)} – Bi – Te^{(1)}$ [12]. An illustration of this structure is seen in Figure 3.1.

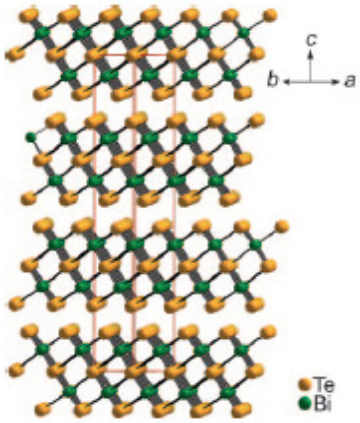


Figure 3.1. Crystal structure of un-doped $Bi_2Te_3$ with five layers stacked in the c-direction by van der Waals forces [13].

This structure allows the crystal to be easily cleaved between the layers. Additionally, impurity atoms can readily occupy interstitial sites between the layers as well as move from one site to another with little energy. This structure also causes many of the properties to be orientation dependent, except for the Seebeck coefficient. In doped $Bi_2Te_3$, this property is independent of orientation and depends on the direction of the temperature gradient instead [13]. Typical operating temperatures for $Bi_2Te_3$ and its alloys range between 300 and 550 K, which is considered the lower end of thermoelectric operating temperatures.

The next intermetallic compound of commercial interest is PbTe, which is the primary thermoelectric material for mid-range temperature (600 to 800K) applications. The crystal structure is much simpler in PbTe, which forms a NaCl structure with Pb atoms in the cation sites and Te in the anion sites. This structure results in isotropic material properties, which makes device fabrication much easier.

Like $Bi_2Te_3$, PbTe can be doped for either n-type or p-type behavior. However, this material does not quite reach the ZT values seen in $Bi_2Te_3$, falling short just short at 0.8 – 1 at 650 K [13].

The final intermetallic compound to be discussed is Si and Ge alloys, which are particularly suited for high temperature (~1200K) applications. Interestingly, Si and Ge are not good thermoelectric materials separately due to their large thermal conductivities. When alloyed together, the resulting thermal conductivity is significantly lower, approximately an order of magnitude lower for some compositions. This large reduction also does not significantly reduce the carrier mobility in the material, allowing for a ZT between 0.6 and 0.8 at its elevated temperatures [14]. Figure 3.2 below compares the figure of merit values versus temperature for some of the most common intermetallic compounds used for thermoelectric application. Note that many of these materials server as baselines for research, and their ZT values can be improved via heavy doping.

**Section 3.2: Complex crystals**

More recently, materials with complex crystal structures have been discovered that offer many areas for future research. This class of materials is typically described as having a phonon-glass/electron crystal (PGEC) behavior. While this description can be used for many other materials that inhibit phonon transport while having little effect on electron transport, it applies best to these materials due to the special structures that arise. In this group of PGECs, cages or

tunnels within the crystal structure hold massive atoms that do not fully occupy the available interstitial space, which allows these atoms to “rattle”. This rattling causes a phonon damping effect that can drastically reduce the thermal conductivity in the material [15].

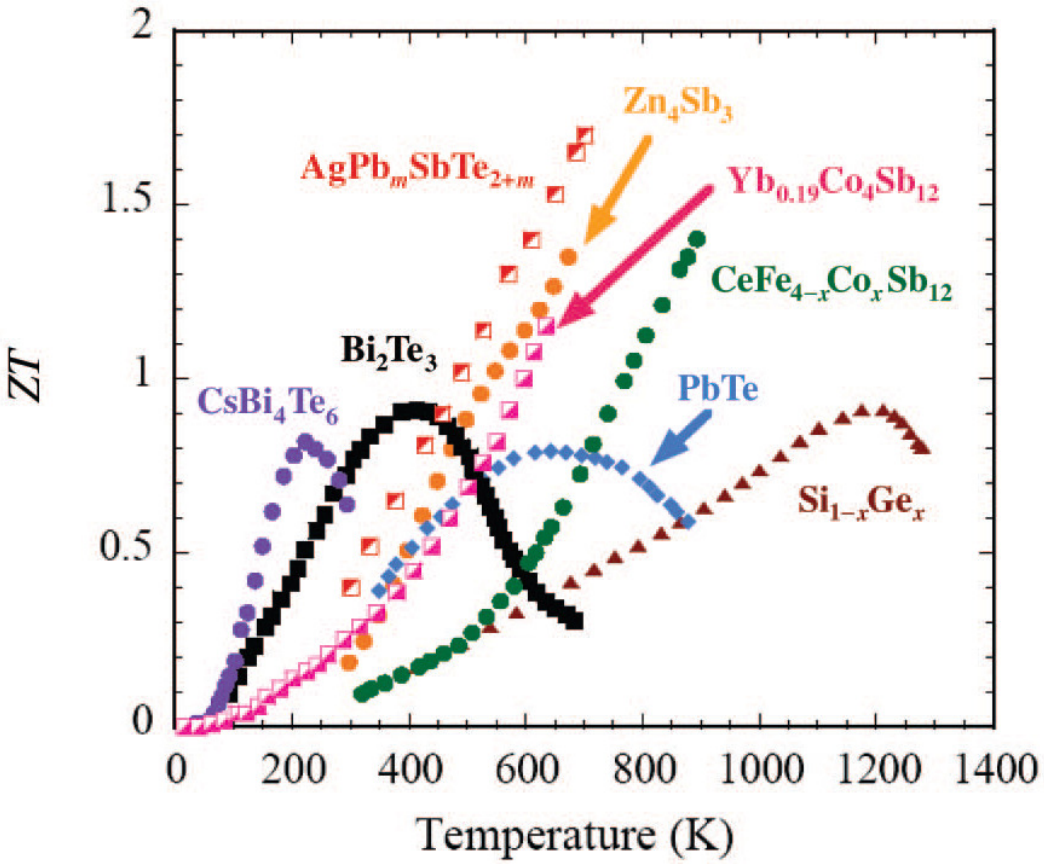


Figure 3.2. Figure of merit, ZT, as a function of temperature for several common intermetallic compounds [14].

One of the most promising and best researched classes of the complex crystals is called skutterudites. These materials are typically binary compounds of

the form $MX_3$ which are then filled with the heavy atom to form a ternary structure $A_xM_4X_{12}$ [16]. An example of this structure is shown in Figure 3.3.

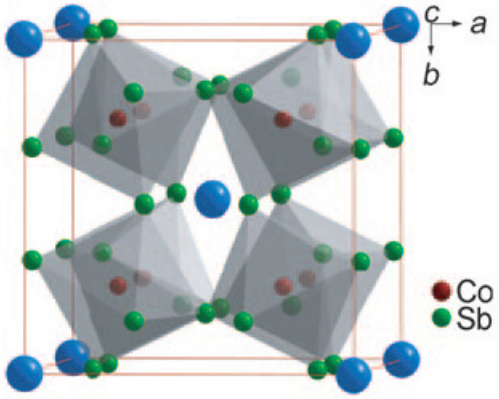


Figure 3.3. This $CoSb_3$ unit cell is an example of a skutterudite structure. The blue spheres illustrate the voids that could be occupied by heavy atoms [13].

Heavy atoms can either act as donors or acceptors, so a wide range of doping criteria can be used to optimize carrier concentrations in order to improve the power factor of these materials. With the reduced thermal conductivity caused by the rattling atoms, these materials are predicted to have relatively high ZT values, with some reports showing ZT values approaching 1.4 above 1000 K [17].

Another class of thermoelectric materials that have complex crystal structures and exhibit strong PGEC behavior is clathrates. Like skutterudites, these materials trap atoms within voids in their structure, but are much more complex. This family of materials derived from binary structures of the form $A_8X_{46}$ (A is alkaline or alkaline earth elements, with X being Si or Ge), which form complex polyhedral shapes

within their crystal structure with element X that are filled with element A atoms [16]. Due to the novel nature of these materials, the data that exists for clathrates is primarily theoretical.

Clathrates primarily come in two types. The more common type, Type I features two different “guest” atoms that fill the two different polyhedral voids. Predictions for certain optimized Type I materials show ZT values around 0.5 at room temperature, and as high as 1.7 at 800 K. Type II clathrates are less common, but do not require that all of their polyhedral voids must be filled like Type I structures. This would allow the properties of Type II clathrates to be tuned by controlling the doping level. Figure 3.4 shows examples Type I and Type II clathrate structures [17].

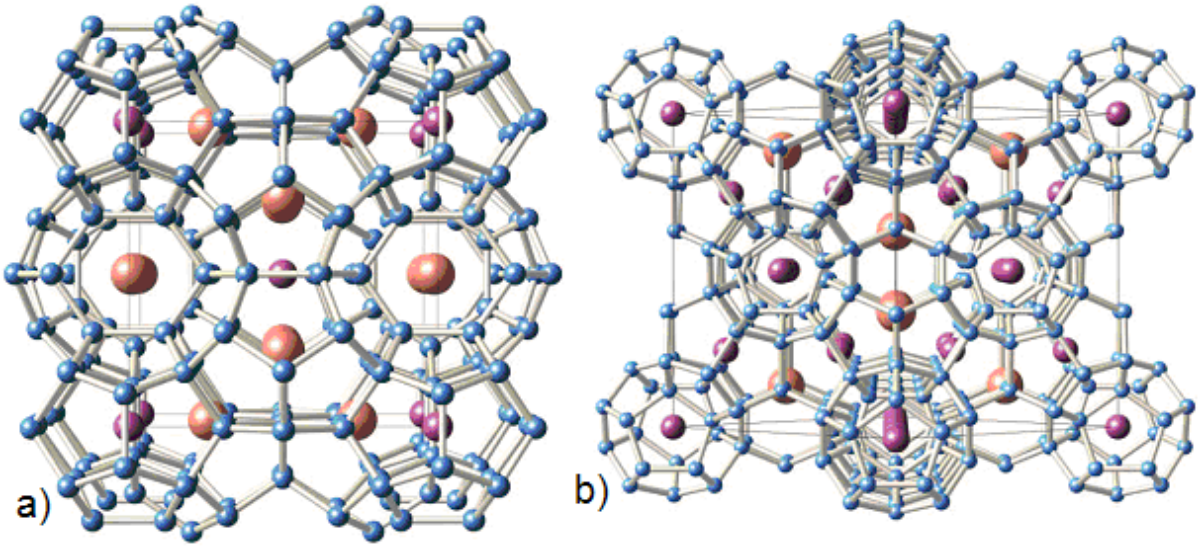


Figure 3.4. Examples of two clathrate structures, (a) being a Type I structure and (b) showing a Type II. Orange and purple spheres are guest atoms with in the polyhedral voids [17].

**Section 3.3: Metal oxides**

One of the newest class of materials to be investigates are metal oxides. As mentioned previously, the high thermal and chemical stability of these oxides makes these very appealing for high-temperature devices placed in air. Initial surveys of these materials proved discouraging due to their lower than expected performance given the starting materials. This low performance is believed to be caused by the high contact resistance at the junction between the oxides and the metal electrodes used for measurements.

Recently, however, certain p-type cobalt oxides have been found to have high power factors coupled with low thermal conductivity which has rekindled research in this class of materials. These layered cobalt oxides consist of sheets of $CoO_2$ sandwiched between sodium layers or misfit layers of calcium cobalt oxide, see Figure 3.5. The $CoO_2$ layers serve as electron transport layers, while the sodium or calcium layers act as phonon scattering regions to lower the thermal conductivity [18]. These cobalt compounds have shown ZT values near 0.8 for polycrystalline samples at 1000 K, and >1 at 800 K for single-crystal samples.

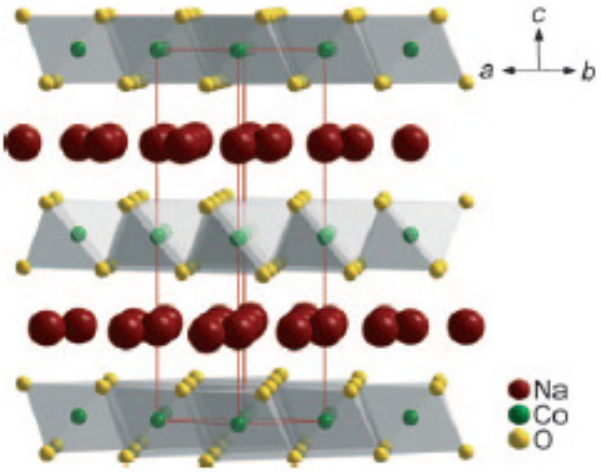


Figure 3.5. Example of the layered structure of the cobalt oxide, $NaCo_2O_4$. The $CoO_2$ layers serve as electron transport regions, while the Na ions act as phonon scattering regions [13].

A corresponding n-type metal oxide showing reasonably good performance is proving much more difficult to discover. While heavily doped $SrTiO_3$ is the current front runner in this category, Al-doped ZnO shows similar ZT values (0.3 at 1000K) [13]. However, ZnO shows promise for improvement due to its simple structure and the wide range of useful materials that have been studied for doping ZnO [1].

**Section 3.4: Nanocomposites**

As noted in the previous sections, past work into improving the thermoelectric properties in existing materials has focused on altering the dopant of the material. However, there are additional methods becoming available through the emerging field of low-dimensional thermoelectricity by using nanoscale materials engineering.

Initially, this field approached the problem from two areas. The first method was to introduce nanoscale constituents that would produce quantum-confinement effects to improve the power factor. The second was to use the large number of internal interfaces found in nanostructures to preferentially reduce the thermal conductivity over the electrical conductivity. Recently, these two methods have begun to converge, with new materials that use nanoscale inclusions to produce short range low dimensionality within the host material [2].

As mentioned in Section 2.4, there are significant difficulties in separating the three components of the figure-of-merit to manipulate them independently. However, by using the this low dimensionality, two methods for increasing the independence of the properties are available: 1) reducing the thermal conductivity more than electrical conductivity through interface scattering, and 2) increasing Seebeck coefficients more than decreasing electrical conductivity though energy filtering, where energy filtering is the inability of a carrier to cross a boundary if its energy is below a certain value [2]. Method one is the most applicable to this study, due to the desire to lower the thermal conductivity of ZnO. The plot in Figure 3.6 shows that this is possible using a theoretical model of a $Si_{1-x}Ge_x$ thermoelectric material with Si nanowires. This plot illustrates that as the volume fraction of Si nanowires increases, the thermal conductivity is reduced, and the smaller the nanowires are, (and consequently, the larger the number of interfaces) the more significant the reduction.

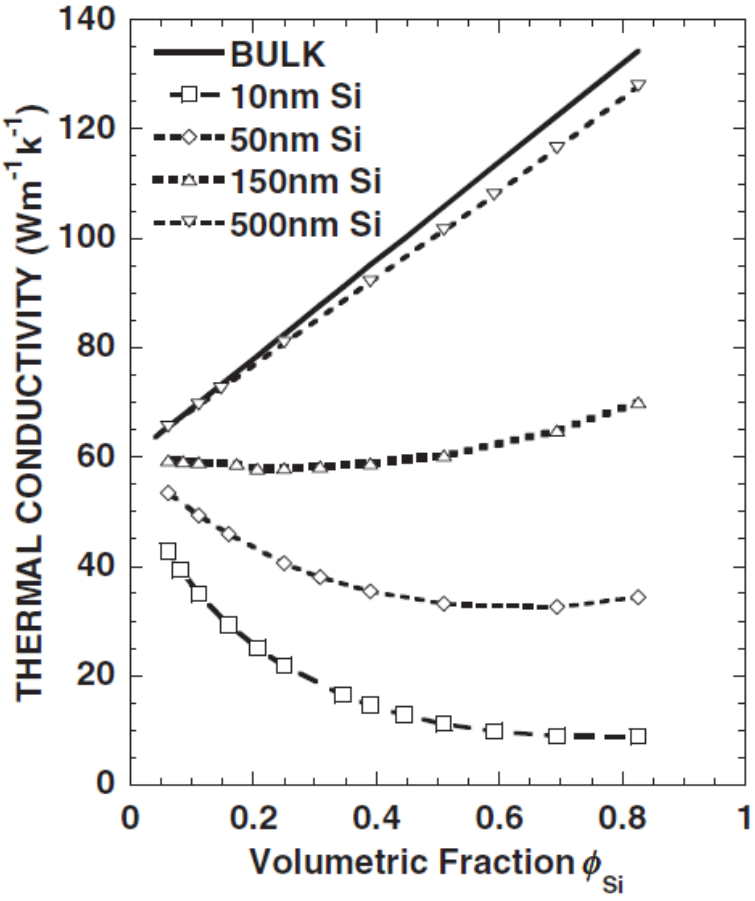


Figure 3.6. Calculated thermal conductivity vs. volume fraction of Si nanowires. The solid line shows the conductivity of a bulk alloy of the same composition [2].

From this chapter, it is clear that the high ZT materials are generally those with some form of complexity in their crystal structures, and by adding complexity to an existing material, ZT can be increased even further. Thus, adding nanoscale inclusions of Cu to ZnO should reduce its thermal conductivity and possibly increase its power factor, ultimately increasing the figure of merit for the material.

# CHAPTER 4

# EXPERIMENTAL METHODOLOGY

## Section 4.1: Material Selection

To create the desired nano-composite, the two constituents materials must meet certain criteria. As mentioned previously, zinc oxide (ZnO) was chosen as the matrix material due to its beneficial properties for high temperature applications. ZnO is thermally stable at higher temperatures, with a melting point at approximately 1975ºC. ZnO is also very chemically stable, showing little to no reactions when exposed to atmospheric conditions at elevated temperatures. Additionally, ZnO has relatively high electrical conductivity across a wide range of temperatures.

For the nano-particle of the composite, this initial investigation is concerned primarily with the density of the material as well as its processing compatibility with ZnO. Copper (Cu) was chosen for this study as it met these criteria. Cu metal is significantly more dense than ZnO, which would provide significant phonon scattering possibilities. In regards to processing compatibility, Cu comes in a number of oxides which all have free energies of formation lower than ZnO [19]. By using this method, ZnO and $Cu_xO$ powders are prepared, and then the $Cu_xO$ compounds can be selectively reduced, leaving ZnO and Cu metal. This circumvents the need to be concerned with the oxidation of Cu metal during the synthesis process.

**Section 4.2: Methodology**

Because this study was the first step in examining copper doped zinc oxide thermoelectric materials, much of the methodology is focused on ceramic processing and characterization techniques. To create the final products to be examined, differing amounts of Copper (II) Oxide (CuO) and Zinc Oxide (ZnO) (Acros Organics 98% pure and Alfa Aesar 99.9% pure respectively) were mixed together, densified, and reduced in specific temperatures and atmospheres in order to selectively reduce the CuO while leaving the ZnO crystals intact.

First, since the desired end result was the dispersion of copper particles within the ZnO crystals, the final volume percentage of copper was used when determining the compositions of the various powder mixtures created. Note that this volume percentage assumes an ideal density in the final product and is likely not perfectly accurate in practice. The volume percent was determined by dividing the desired volume of copper in the final sample by the total volume of the final sample, which is the sum of the copper and ZnO volumes. A wide range powder mixtures was created during this study from 0.25 to 10 volume percent Cu, but most work was done on the 0.25%, 1%, 5%, and 10% mixtures. These volume percentages were then used to determine the final mass of copper in the material. Assuming no oxygen would be reduced from the ZnO, the only mass loss in the material would be from the reduction of CuO. Using this assumption, the initial masses of CuO and ZnO powders were then determined.

Next, the weighed powders were then wet milled to homogenize the distribution of CuO in the mixture. In this step, the powder was milled with yttria stabilized zirconia balls for approximately 4 hours in an isopropyl alcohol solution. Once the milling was complete, the slurry was set out to allow the isopropyl alcohol to evaporate out of the solution. The now dry powder mixture was ball milled without a liquid solution for another 2 hours to reduce the average grain size.

To improve the density of the final samples, the powder mixtures were "pre-reacted" by sintering the loose powder in a 1200℃ furnace (Sentro Tech 1500C-458 High Temperature box furnace) for 12 hours to bond the ZnO and CuO powders and form a better solid solution. The powders were then milled again in a high-energy shaker mill for 2 hours to pulverize the powder and significantly reduce the grain size.

The pre-reacted powders were then uniaxially pressed into pellets 0.5 inch (13 mm) in diameter and 1-2 mm thick at a variety of pressures from 145 MPa to 440 MPa. These pressures were tested to determine the best possible green density of the samples without forming cracks. The pellets were once again sintered in the box furnace at 1200℃ for up to 12 hours with heating and cooling rates of approximately 4℃ per minute. This sintering process would further densify the pellets before the reduction step.

The sintered pellets were then placed in a range of atmospheres in order to selectively reduce the CuO in the material. While the Ellingham diagrams for ZnO and CuO were consulted for the ideal partial pressures of oxygen required to reduce CuO only, the facilities available were unable to maintain the desired partial

pressures. To circumvent this, a variety of gas atmospheres, reduction times (3 to 8 hours), and temperatures (700℃ to 1000℃) were tested to produce the desired results. The atmospheres tested include a variety of vacuum pressures, pure nitrogen, pure forming gas (1% $H_2$, 99% $N_2$), "bubbled" forming gas (gas is passed through water before entering the furnace chamber), and forming gas/$N_2$ mixtures. All non-vacuum reductions were performed in a tube style furnace (Protherm, model PTF 12/75/600). The ideal conditions were determined to be a 1 to 3 mixture of nitrogen to forming gas for 8 hours at 700℃. At each step in the process, the bulk densities of the pellets were calculated using the Archimedes method.

Before and after the reduction process, the crystalline phases in the material were identified using an X-ray diffractometer (Empyriean Cu LFF-HR DK31925) using Cu Kα radiation to compare the amount of Cu present before and after reduction. 2θ-ω scans from 30 to 80 degrees were preformed to capture the peaks of interest for the materials present. Based on the X-ray results, select samples were prepared for transmission electron microscopy (TEM). Standard TEM polishing was performed using diamond lapping films (on an Allied High Tech Multiprep) and then finished using ion milling (on a FIschione Model 1050 TEM mill). Finally, the samples microstructural characteristics were examined using a TEM (JEOL 2000FX S/TEM).

# CHAPTER 5

# RESULTS AND DISCUSSION

As mentioned previously, this investigation is a first step into Cu doped ZnO and so the results discussed here are focused on characterizing the composition and structure of this material using X-ray diffractometry (XRD) and transmission electron microscopy (TEM).

## Section 5.1: Selective reduction of CuO

The first goal of this study was to prove that CuO could be selectively reduced in a bulk ZnO sample. This was accomplished by XRD and mass loss analysis of samples processed under a wide range of conditions. Initial tests were performed on high Cu percentage samples (10 volume percent) so mass losses and x-ray peaks would be easily verifiable.

After determining the desired partial pressure of oxygen to reduce CuO only, a vacuum furnace was first used to reduce sample. This proved to be unreliable due to instrument limitations in maintaining the required vacuum pressure. Next, different atmospheres of $N_2$ and forming gas (FG) were tested. First, pure $N_2$ and pure FG were tested at 1000°C for 10 hours. Such a long time was picked to determine if any kind of equilibrium state could be reached in the samples, which proved to not be the case. Figure 5.1 shows the XRD results of this test.

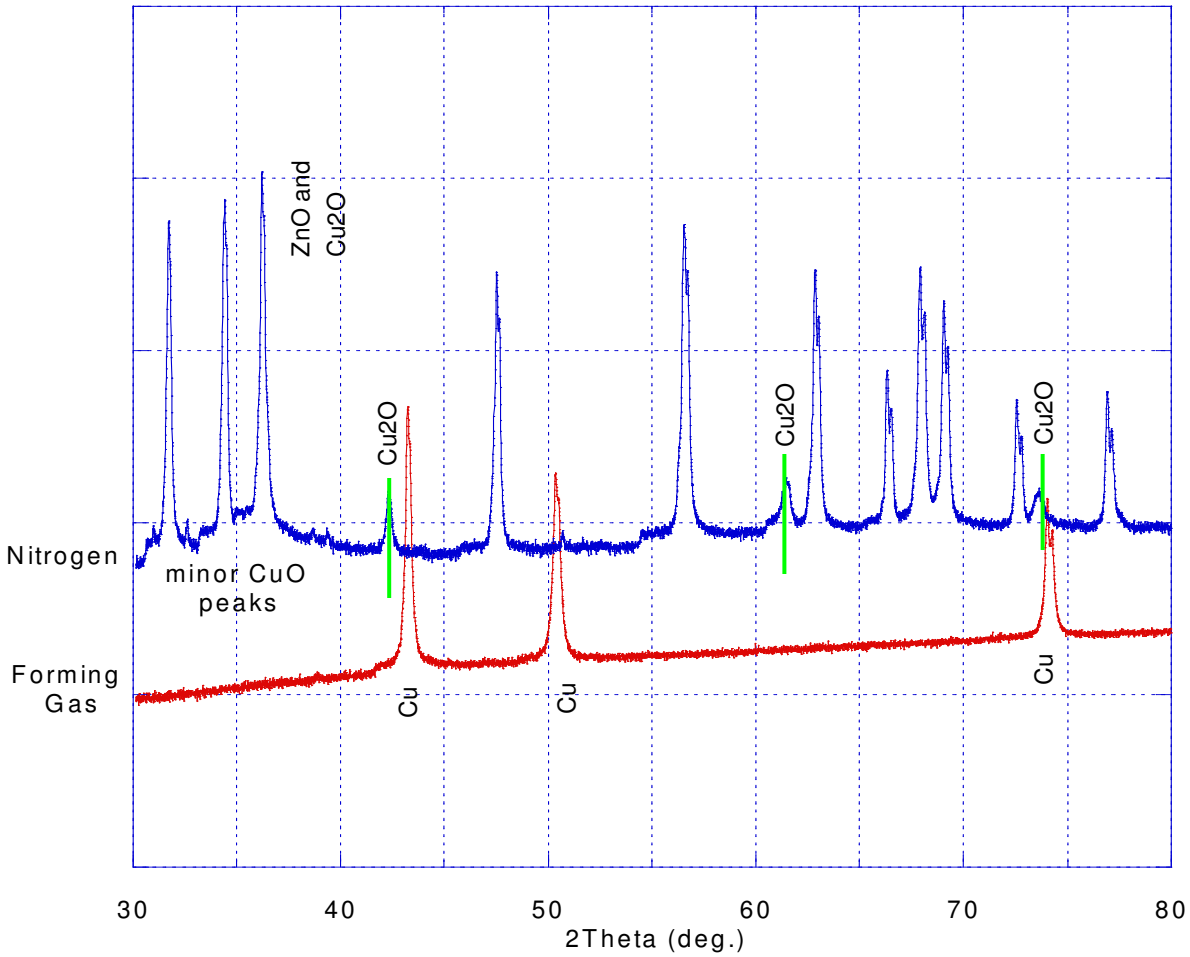


Figure 5.1. XRD plot for samples reduced in pure forming gas and pure nitrogen atmospheres.

From this it is clear that pure $N_2$ proved too weak for reducing CuO completely to Cu. More importantly, this atmosphere also illustrates a hurdle that needs to be overcome when reducing CuO. CuO will easily reduce to $Cu_2O$, which is much more stable than CuO and therefore much more resistant to reduction [19]. In the above plot, nearly all the CuO was converted to $Cu_2O$, with only small remnants of the major peaks still visible.

On the other hand, pure FG is too harsh of an environment as all of the oxygen was reduced from both ZnO and CuO, ultimately removing 93% of the sample mass. This does confirm that no Zn remained in the material, meaning any Zn remaining after reduction evaporated rather than bond with Cu. This shows that in the final result, the particles remaining in the ZnO bulk will be pure Cu, rather than a Cu-Zn alloy. This evaporation of Zn appears counter intuitive at first glance, as one would expect Zn to remain after reduction. However, after consulting a plot of the vapor pressure of the ZnO system (see Figure 5.2), this cause of this result is clear.

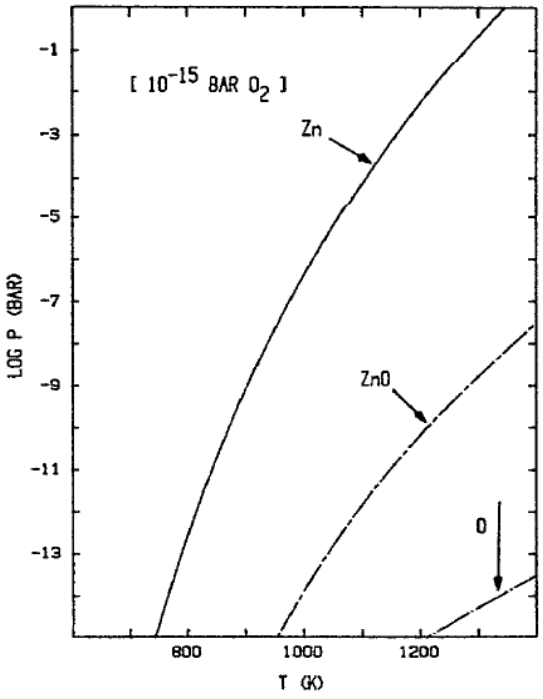


Figure 5.2. Plot of the vaporization pressures of the ZnO system at low partial pressures of oxygen [20].

This figure shows that at significantly low partial pressures of oxygen, such as in the forming gas reducing conditions, the vaporization pressure of Zn is significantly lower than ZnO. Due to the fact that the reductions are performed in an open system, any Zn that is vaporized from the sample is then swept away from the sample. This allows more Zn to be vaporized from the sample. And this process continues until all the Zn is removed from the system.

Clearly, a mixture of $N_2$ and FG should produce the desired reduction conditions, where CuO is reduced, but the evaporation of Zn is minimized. Many mixtures were tested at a variety of reduction times and temperatures, from 100:1 to 1:6 $N_2$ to FG, but ultimately more detailed investigations were performed on the two most promising mixtures: 1:3 and 3:1 $N_2$ to FG (smaller ratios were unable to be tested due to instrument limitations). These gas mixtures were tested against a large range of temperatures (1000°C to 600°C) and times (3 to 10 hours). These results are shown in the following figures.

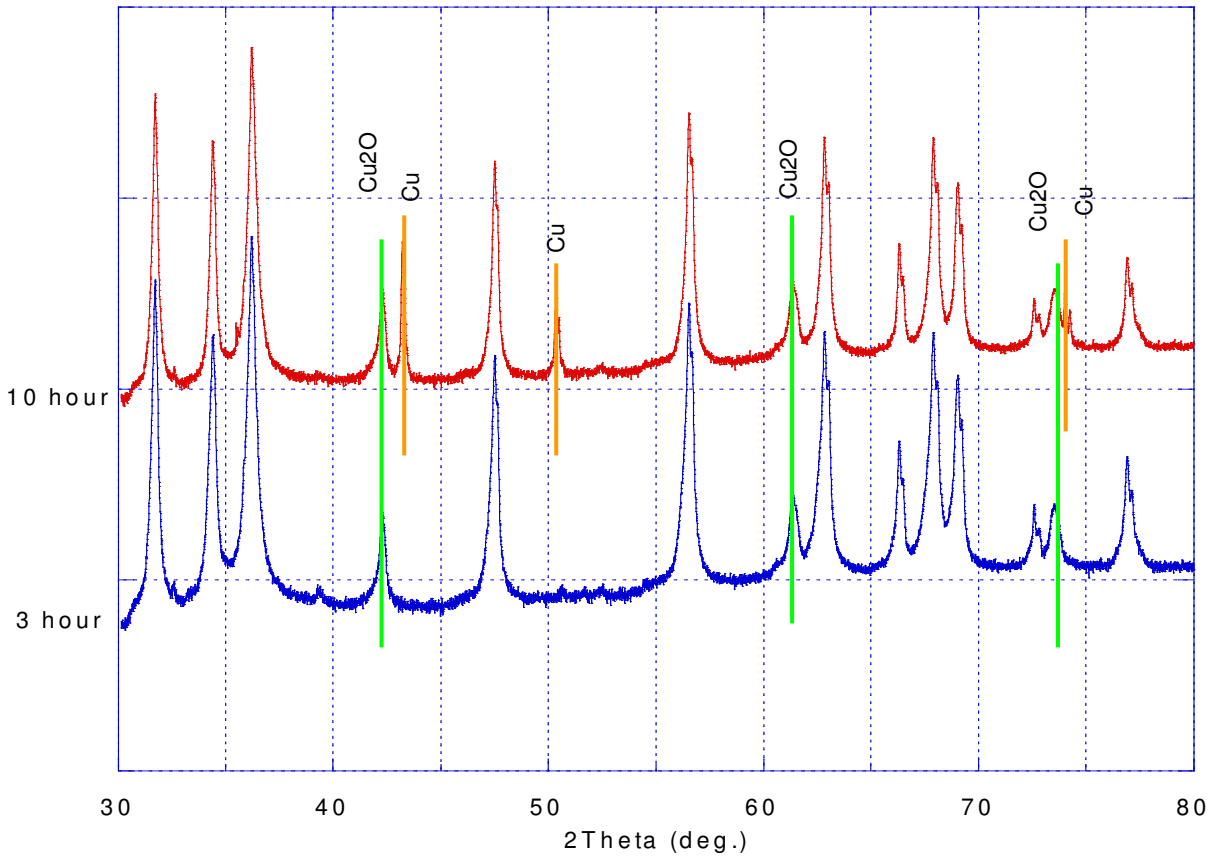


Figure 5.3. XRD plot showing the reduction in a 3:1 N2:FG atmosphere at 1000℃ at 3 hrs and 10 hrs.

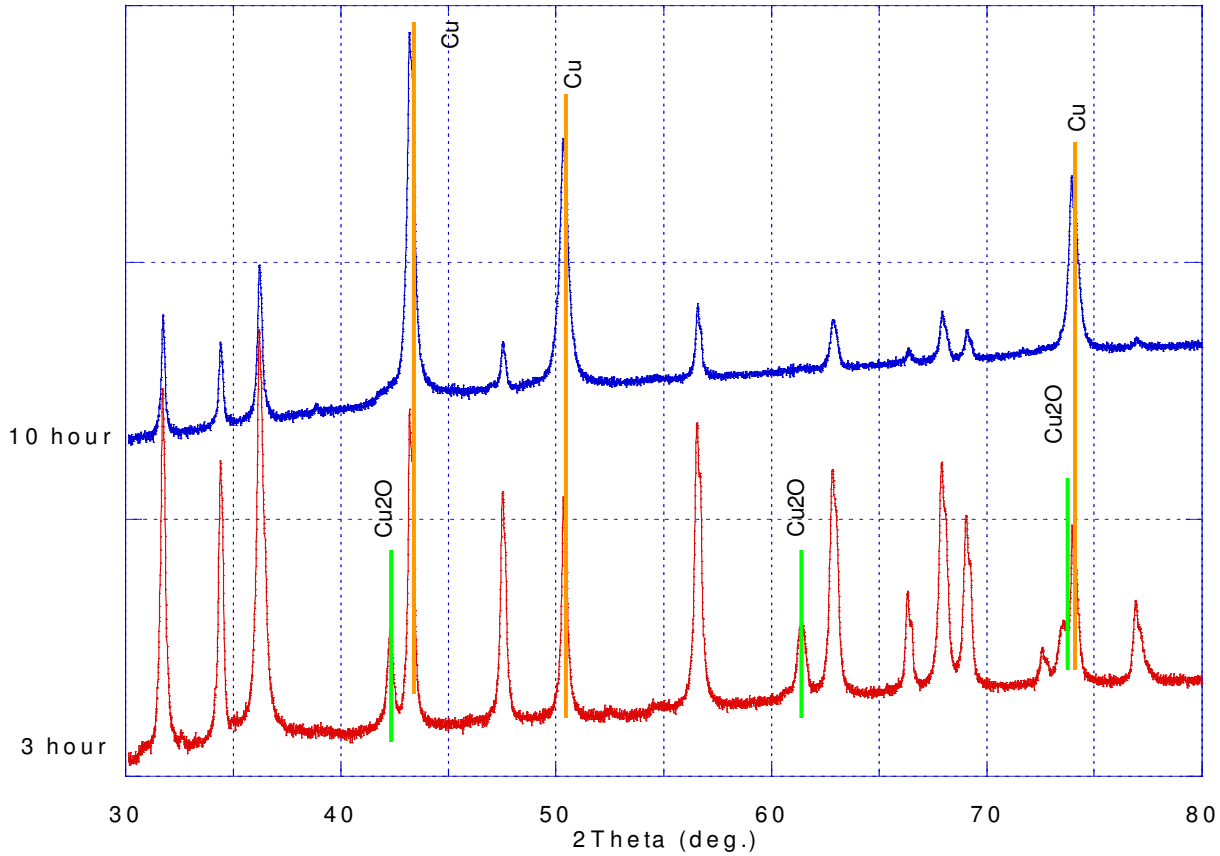


Figure 5.4. XRD plot showing the reduction in a 1:3 N2:FG atmosphere at 1000℃ at 3 hrs and 10 hrs.

This test quickly ruled out the 3:1 mixture. Even at the high temperature, additional reduction does not occur after 5 hours. At this point, the 3:1 gas mixture was abandoned, and focus was placed on the 1:3 gas mixture.

While 1000℃ is too high of a temperature, causing significant reduction and evaporation of ZnO from the sample, the longer reduction time is apparently needed for the system to completely reduce the CuO present. Therefore, this long time was maintained, and lower temperatures were tested, as seen in the following figures.

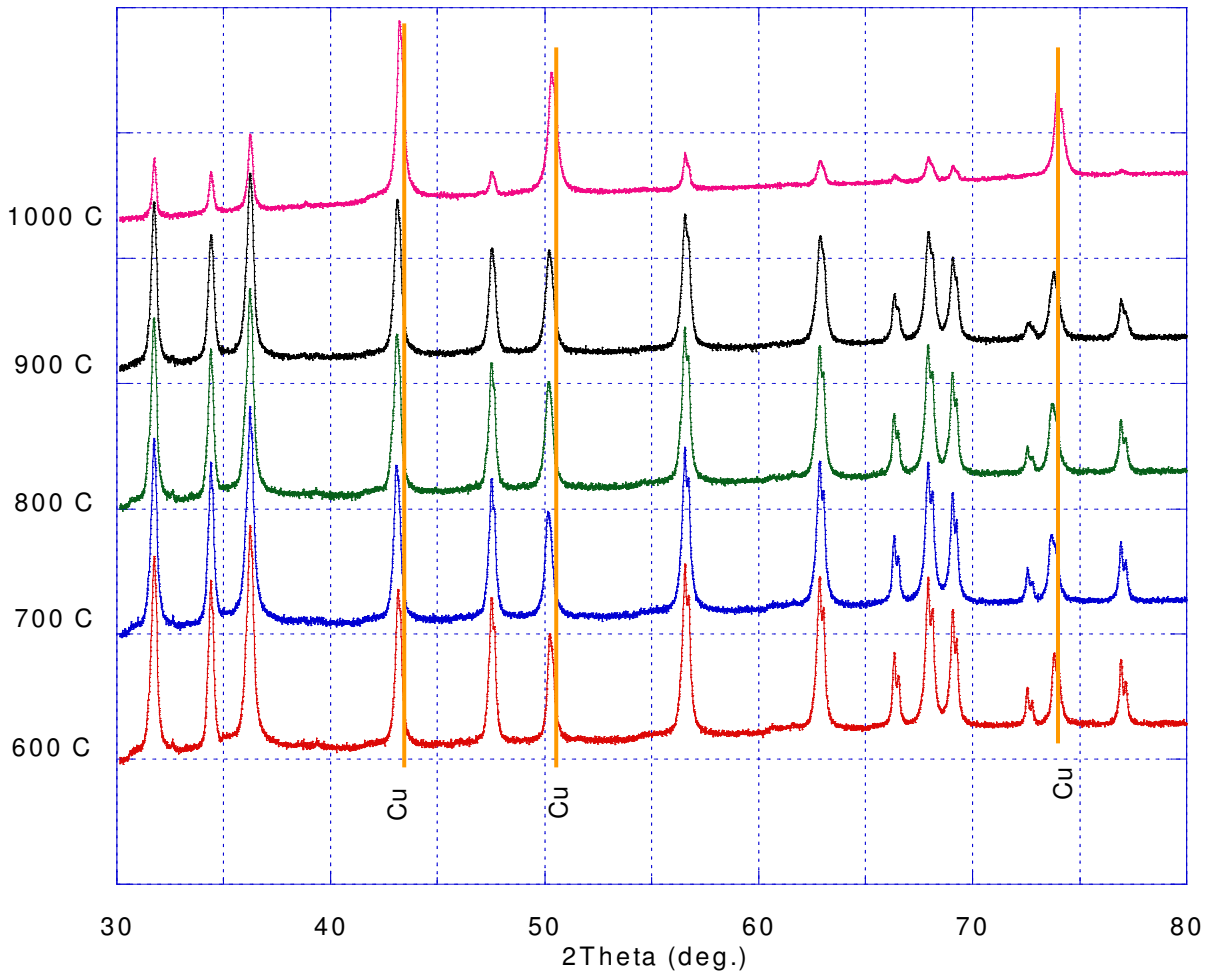


Figure 5.5. XRD plot showing the reduction in a 1: 3 $N_2$:FG atmosphere for 10 hours at temperatures from 600 to 1000℃.

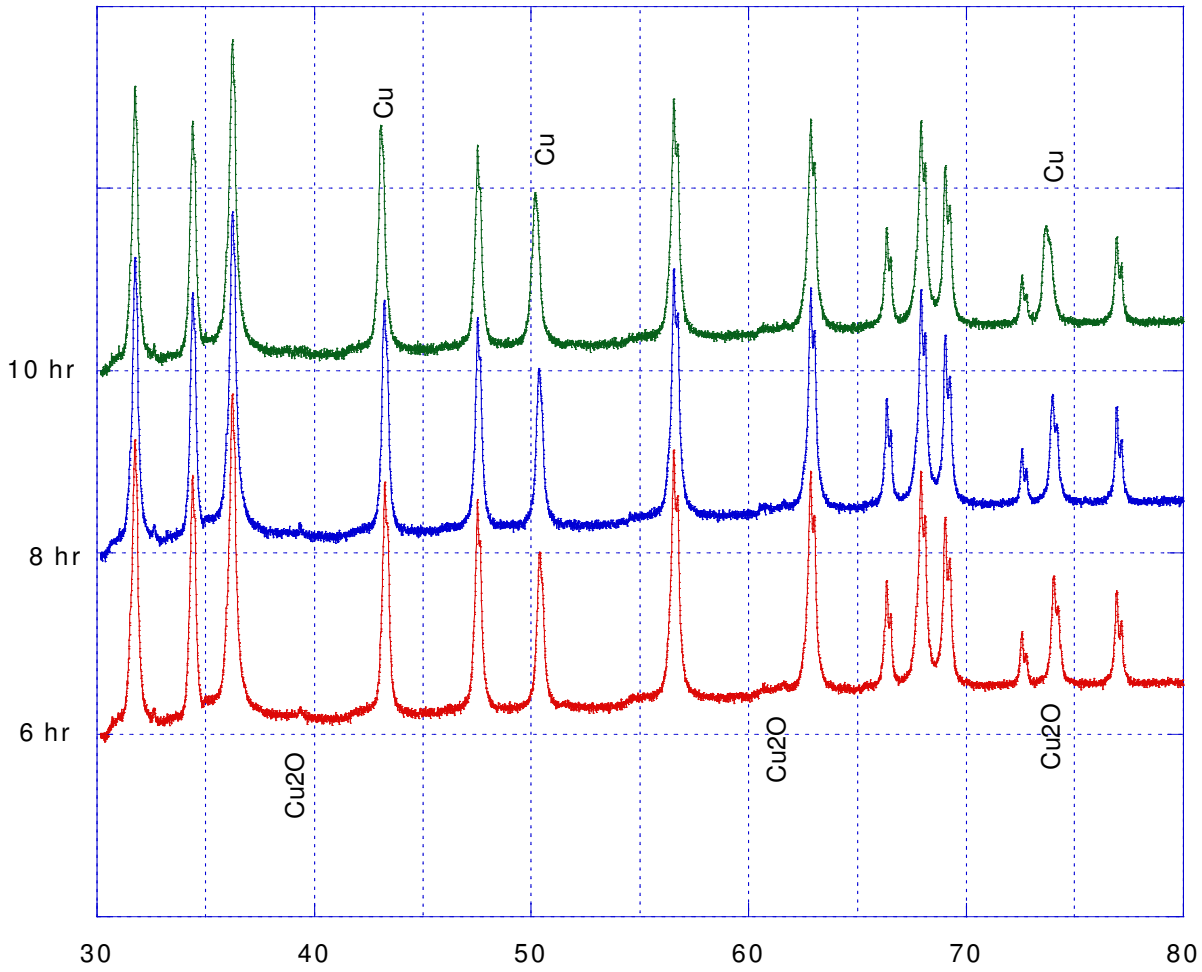


Figure 5.6. XRD plot showing reduction in a 1:3 $N_2$:FG atmosphere at 700℃ for various times.

Figure 5.5 shows that insignificant reduction improvements took place at lower temperatures, maintaining a full reduction of CuO to Cu. However, as the ZnO peaks illustrate, significant amounts of ZnO was lost at higher temperatures, while leveling off between 800℃ and 700℃. Figure 5.6 shows that no significant improvement was seen after 8 hours. Therefore, the final reduction conditions for

the selective reduction of CuO were determined to be a 1:3 mixture of $N_2$ to forming gas at 700℃ for 8 hours.

**Section 5.2: TEM characterization**

Prior to TEM characterization, the density of the samples needed to be improved. Even a small amount of CuO proved to have a large negative effect on the densification of ZnO, reducing the final theoretical density of the sample pellets by approximately 10% for the smallest Cu volume percentage and up to 20% at higher Cu volume percentages. Using pre-reacted powders, high-energy shaker milling, and higher sintering temperatures, theoretical densities for the final reduced samples of approximately 85% were achieved, and an improvement of approximately 15% for the worst cases. While not fully densfied, these densities were sufficient for TEM analysis. Any further analysis outside of the scope of this study may require higher sample densities, which could be achieved using more advanced processing techniques, such as isostatic pressing.

Pellets with compositions ranging from 0.25% to 10% Cu by volume were prepared for TEM analysis. The process used to create these pellets is outlined in Chapter 4, and were reduced using the parameters discussed in the previous section. During the polishing stage, large amounts of Cu were observed accumulating outside the ZnO grains for volume percents starting at 5%. Due to this undesirable condition, three compositions were selected for further preparation and analysis: 5%, 1%, and 0.25% Cu by volume.

First, the 5% sample was analyzed. Representative images of this sample are shown in the following group of figures.

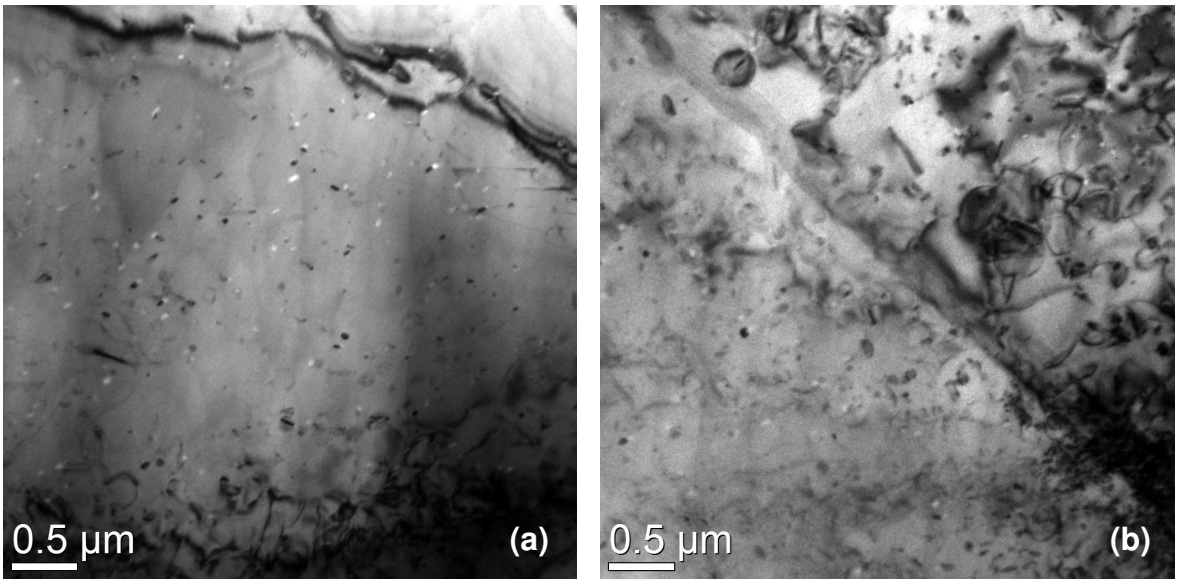


Figure 5.7. These images show the typical particle distribution. (a) shows was taken in the middle of a ZnO grain, while (b) shows a nearby grain boundary

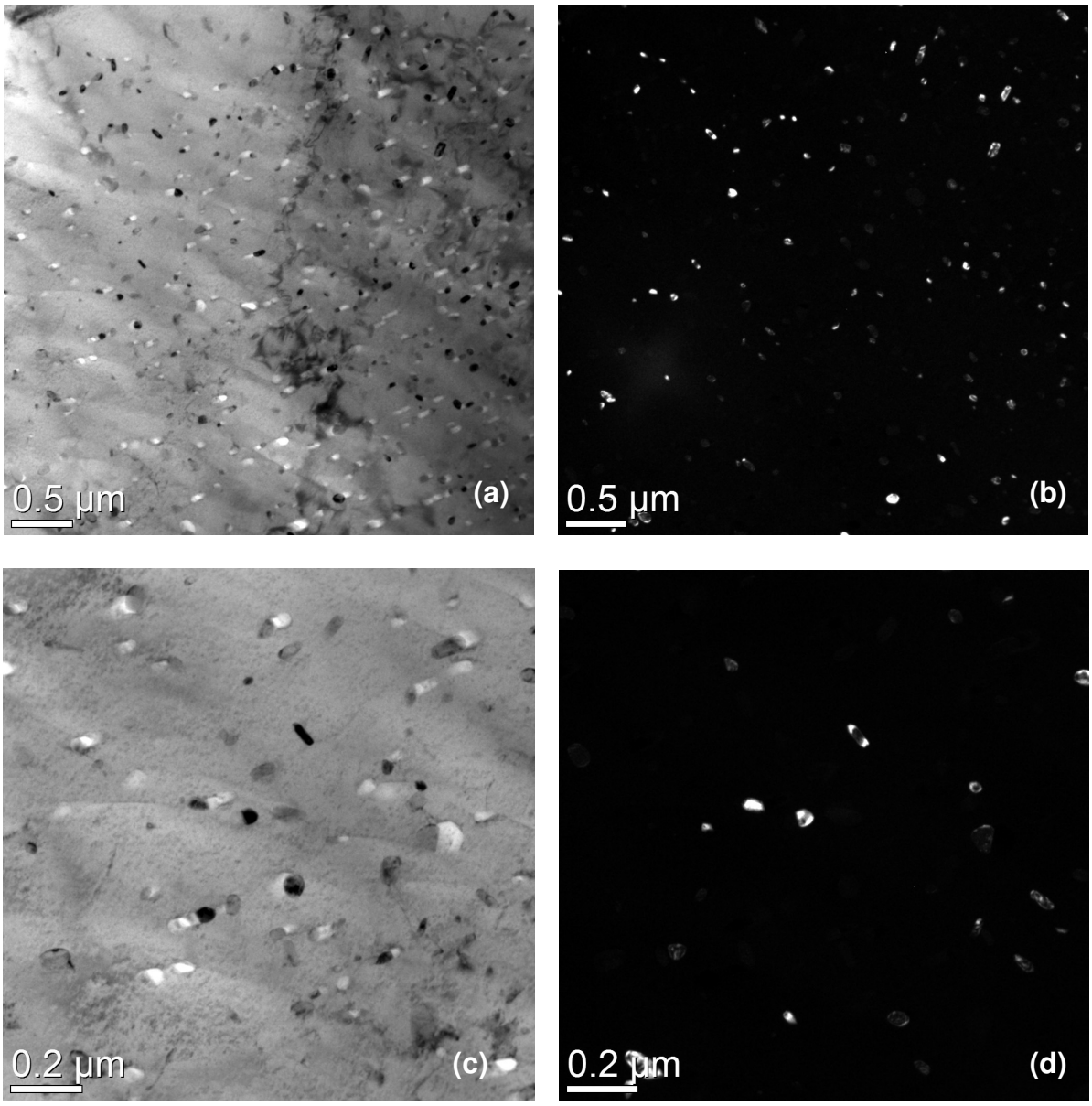


Figure 5.8. These images which highlight the particles present within a grain. (a) and (b) are bright and dark field images respectively at low magnification. (c) and (d) are the same regions, but at higher magnification.

These images show the typical distribution of particles in these samples. The first thing to notice is that the particles are evenly distributed throughout the material.

Figures 5.7a and 5.7b show that the particles do not congregate on grain boundaries or clump together. At the higher magnification, the shape of the particles is clear. The particles form either rods or spheres (which may be rods viewed on-axis) with a length between 100 and 200 nm and width or diameter of approximately 30 nm. This size and shape is fairly regular throughout. In Figure 5.8, many light spots are present, and appear to be roughly in the shape of the surrounding particles, and do not appear in the dark field images. These spots are believed to be holes left in the material when a copper oxide particle is reduced to Cu metal. The transition from CuO to Cu is accompanied by a density reduction of approximately 56%. This is shown by the particles which have light spots forming around them which are roughly half filled. The empty holes could correspond to where Cu had diffused to other Cu particles, which potentially explains why there are particles with no voids beginning around them.

Accumulated copper that appeared to be present after polishing was not visible after ion milling, which due to the fairly high porosity was anticipated. Much like the small Cu particles were milled out, the larger accumulations would have fallen free as the pores were grown during milling. With more rigorous powder processing, these copper grains could be possibly be eliminated.

Next, the 1% samples were evaluated. Images from these samples are shown in the following figures:

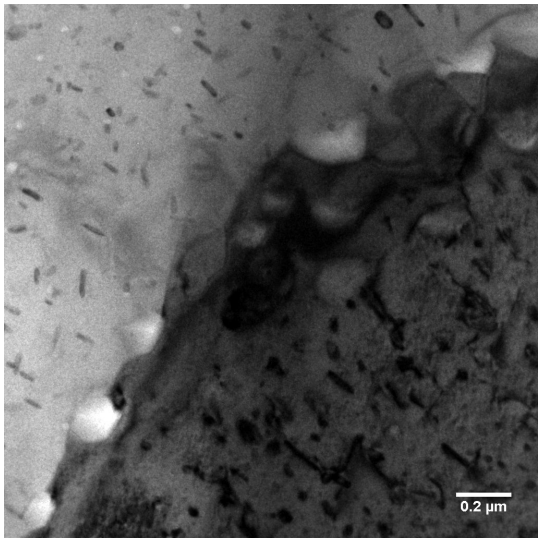


Figure 5.9. Again showing the regular distribution and shape of Cu particles at a low magnification.

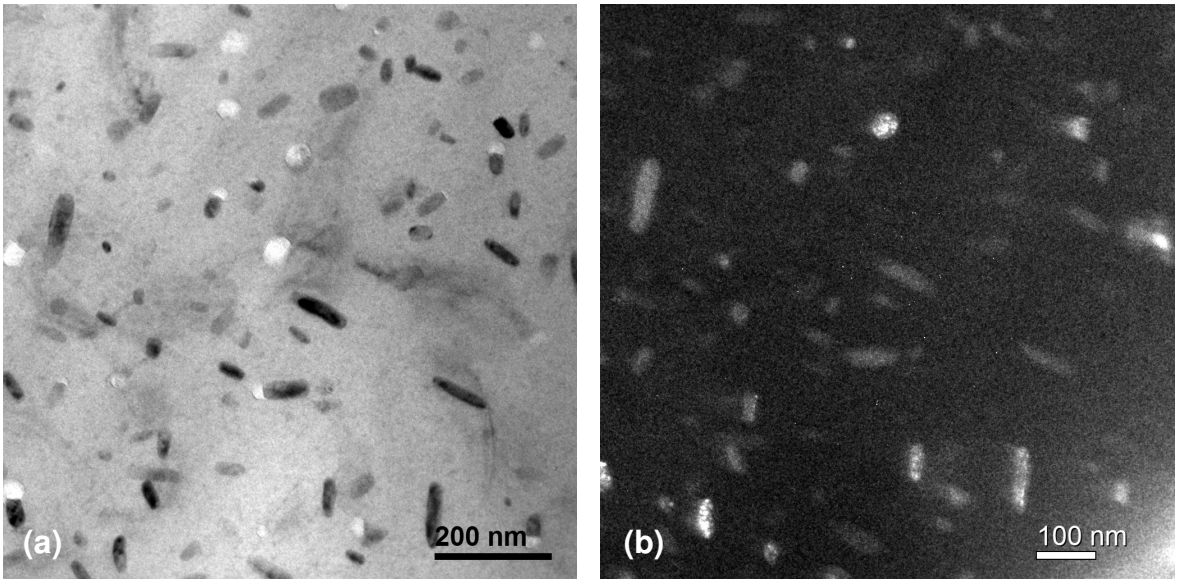


Figure 5.10. (a) and (b) are bright and dark field images respectively at higher magnification.

Once again, the even distribution of particles is present. Interestingly, the number, size, and shape of the particles appear very similar to that of the 5% sample if slightly reduced. This could be due to a saturation of Cu or CuO within the ZnO grains which caused the precipitation of excess Cu outside of the ZnO as seen in the 5% samples. This even distribution and common particle shape would for providing regular phonon scattering sites for decreasing thermal conductivity

Finally, the 0.25% samples were imaged and the results are seen in the following figures:

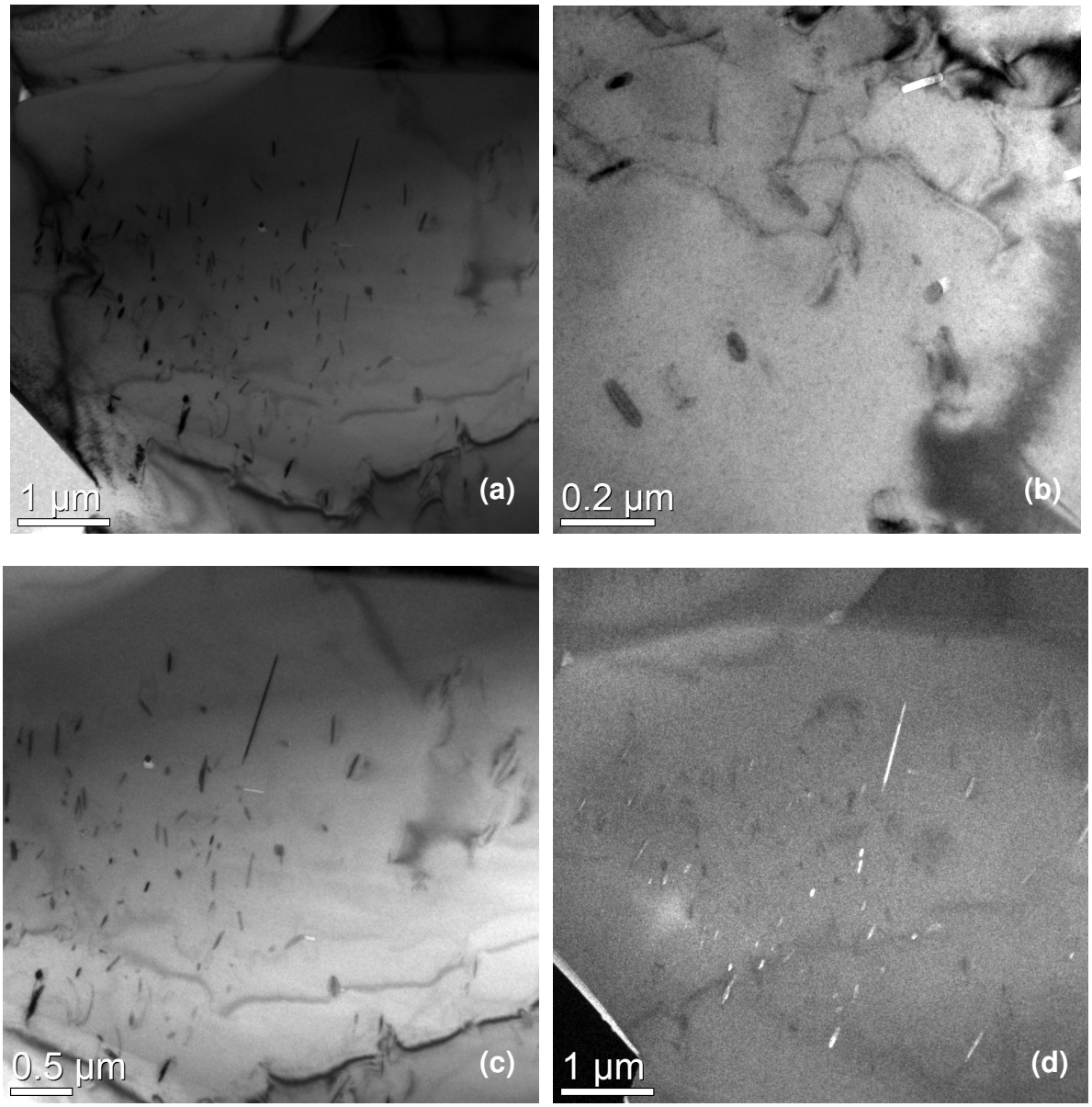


Figure 5.11. These images still show regularly spaced particles, but are more sparsely and unevenly distributed. (a) and (b) show low and high magnification images of typical particle groups, where (c) and (d) show bright field and dark field images of these particles in better detail.

These figures show rather intriguing differences from what was seen in the previous samples. While the general rod-like shape of the particle remains and the

rough distribution is similar, they are much narrower than previous samples. The distribution of particles is also less regular than in the higher percent samples. This is to be expected due to the lower copper content in these samples and processing artifacts.

**Section 5.3: Preliminary thermal property measurements**

Some preliminary results were able to be obtained with the help of Dr. Patrick Hopkins at the University of Virginia. Sample of the same compositions investigated in TEM (0.25%, 1%, and 5%) were polished and sent for thermoreflectance measurements in order to determine their thermal conductivities.

Despite the porosity of the samples (~85% for each) the measurements performed by Dr. Hopkins included statistical modeling to determine the conductivity of the crystals only. This allows for a direct comparison to the thermal conductivities of pure, bulk ZnO (~52 W/m/K) as a reference point.

The results obtained were: 42.6±15.4 W/m/K, 17.3±6.1 W/m/K, and 14.8±5.6 W/m/K for the 0.25%, 1%, and 5% samples respectively. These results are plotted in Figure 5.13.

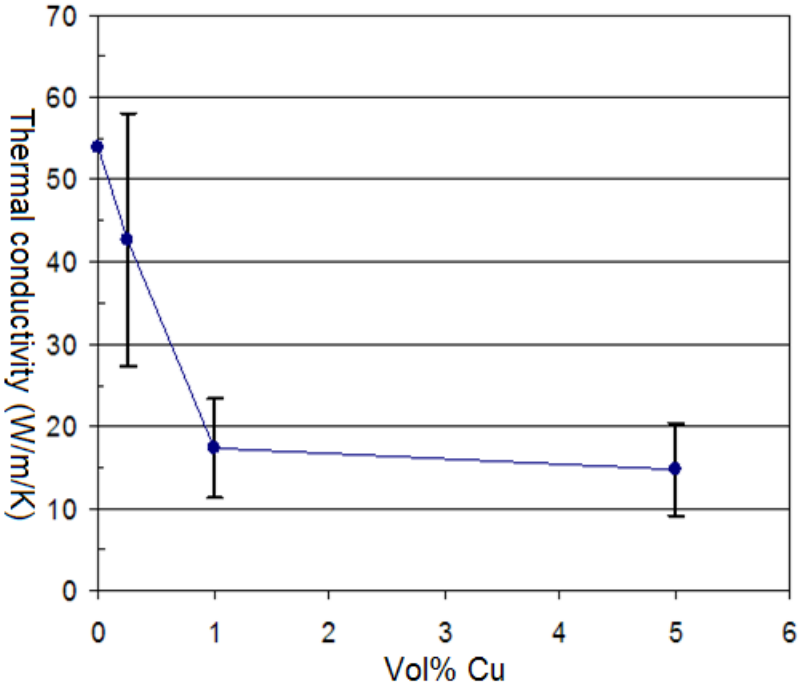


Figure 5.12. Plot of thermal conductivity of bulk ZnO-Cu samples at a variety of volume percents of Cu

From this figure we can see that a significant reduction in thermal conductivity was obtained. Additionally, when compared to Figure 3.6, we see the expected curve shape of the smaller nanoparticle size (<150nm), showing that the reduction in conductivity is being influenced by the addition of the Cu nanoparticles.

# CHAPTER 6

# CONCLUDING REMARKS

From this study, we concluded that the production of a nano-composite of Zno and Cu metal is possible using the selective reduction of CuO. Through careful control of the processing and reducing conditions and sample compositions, nano-structures within the material are spontaneously created without the need for direct material processing. Preliminary results show that a reduction in thermal conductivity is achieved, and the reduction is shown to improve with increasing volume percentage of Cu particles.

Further measurements should be done to confirm these thermal property enhancements, as well as to determine the effect on the other terms in the figure-of-merit equation: electrical conductivity and Seebeck coefficient. Future study in this area could investigate the effect of using doped ZnO which would enhance the electrical conductivity of the matrix.

## REFERENCES


1: Tanaka, Y.; Ifuku, T.; Tsuchida, K.; Kato, A., Thermoelectric properties of ZnO-based materials. *Journal of Materials Science Letters* **1997**, 16, 155-157.

2: Dresselhaus, M. S.; Chen, G; Ming, Y. T.; Yang, R.; Lee, H.; Wang, D.; Ren, Z.; Fleurial, J.; Gogna, P., New Directions for Low-Dimensional Thermoelectric Materials. *Advanced Materials* **2007**, 19, 1043-1053.

3: Saber, H. H.; El-Genk, M. S.; Caillat, T., Tests Results of Skutterudite Based Thermoelectric Unicouples. *Energy Convers. Manage.* **2007**, 48, 555-567.

4: Koumoto, K. *Oxide Thermoeletrics*. Research Signpost, Trivandrum, India. 2002.

5: Kim, K. H.; Shim, S. H.; Shim, K. B.; Niihara, K.; Hojo, J., Microstructural and Thermoelectric Characteristics of Zinc Oxide Based Thermoelectric Materials Fabricated Using a Spark Plasma Sintering Process. *Journal of the American Ceramic Society* **2005**, 88 [3], 628-632.

6: Snyder, G. J.; Toberer E. S., Complex thermoelectric materials. *Nature Materials* **2007**, 7, 105-114.

7: Rowe, D. M., Introduction. In D.M. Rowe (Ed.) *CRC Handbook of* Thermoelectrics. Boca Raton, FL: CRC Press. 1995.

8: Emin, D., Effects of Charge Carriers' Interactions on Seebeck Coefficients. In D.M. Rowe (Ed.) *Thermoelectric Handbook: Macro to Nano*. (pg. 5-1 to 5-7). Boca Raton, FL: Taylor & Francis Group, LLC. 2006

9: Rowe, D. M., General Principles and Theoretical Considerations. In D.M. Rowe (Ed.) *Thermoelectric Handbook: Macro to Nano*. (pg. 1-1 to 1-14). Boca Raton, FL: Taylor & Francis Group, LLC. 2006

10: Bilc, D. I., *Electronic and Transport Properties of Novel Thermoelectrics.* VDM Verlag Dr. Muller Aktiengesellschaft & Co. KG. 2009.

11: Tritt, T. M.; Subramanian, M. A., Thermoelectric Materials, Phenomena, and Applications: A Bird's Eye View. *MRS Bulletin*. **2006**, 31, 189.

12: Scherrer, H.; Scherrer, S., Bismuth Telluride, Antimony Telluride, and Their Solid Solutions. In D.M. Rowe (Ed.) *CRC Handbook of* Thermoelectrics. Boca Raton, FL: CRC Press. 1995.

13: Sootsman, J. R.; Chung, D. Y.; Kanatzidis, M. G., New and Old Concepts in Thermoelectric Materials. *Angewandte Chemie International Edition* **2009**, 48, 8616-8639.

14: Tritt, T. M.; Subramanian, M. A., Thermoelectric Materials, Phenomena, and Applications: A Bird's Eye View. *MRS Bulletin*. **2006**, 31, 188-194.

15: Goldsmid, H. J. *Introduction to Thermoelectricity*. New York, NY. Springer Heidelberg Dordrecht. 2009

16: Godart, C.; Goncalves, A. P.; Lopes, E. B.; Villeroy, B., Role of Structures on Thermal Conductivity in Thermoelectric Materials. *Properties and Applications of Thermoelectric Materials*. **2009**, 19-49.

17: Nolas, G. S.; Poon, J.; Kanatzidis, M., Recent Developments in Bulk Thermoelectric Materials. *MRS Bulletin*. **2006**, 31, 199-205.

18: Koumoto, K.; Terasaki, I.; Funahashi, R., Complex Oxide Materials for Potential Thermoelectric Applications. *MRS Bulletin*. **2006**, 31, 206-210.

19: Gaskell, D. R., *Introduction to the Thermodynamics of Materials*. New York, NY: Taylor & Francis. 2003.

20: Lamoreaux, R.H.; Hildenbrand, D. L., High-temperature Vaporization Behavior of Oxides II. Oxides of Be, Mg, Ca, Sr, Ba, B, Al, Ga, In, Tl, Si, Ge, Sn, Pb, Zn, Cd, and Hg. *J. Phys. Chem. Ref. Data*. **1987**, 16, 419-443